J Fail. Anal. and Preven. (2019) 19:1792–1800
https://doi.org/10.1007/s11668-019-00780-1

TECHNICAL ARTICLE—PEER-REVIEWED

Improvement in Accuracy of Failure Prediction in Sheet Hydroforming of Square Cups Using Stress-Based Forming Limit Diagram

Nilesh Gajjar · Bharatkumar Modi · Ravi Kumar Digavalli

Submitted: 5 July 2019 / in revised form: 12 August 2019 / Published online: 28 October 2019

Abstract Prediction of failure in sheet metal forming processes accurately is very important for successful production and optimization of parameters. A major problem of conventional strain-based forming limit diagrams (FLDs) is their inability to predict failure accurately in processes such as sheet hydroforming where there is a change in strain path and mode of deformation. In the present work, a stress-based forming limit diagram has been developed for AA 5182 alloy sheets modifying the analytical procedure, proposed by Stoughton, to determine forming limits in stress space from failure strains incorporating anisotropy using Balart's yield criterion. The developed stress-based FLD has been used to predict failure in sheet hydroforming of square cups. Results are compared with Hill's quadratic yield criterion. Significant difference has been found in failure prediction between strain-based and stress-based criteria when they are applied to sheet hydroforming. A change in strain path has been observed at the critical corner regions in hydroforming of square cups due to initial drawing and then biaxial stretching during calibration. The experimental validation clearly showed that accuracy in failure prediction can be improved in sheet hydroforming by using a stress-based forming limit diagram.

Keywords Hydroforming · Aluminum alloy · Failure prediction · Forming limit diagram

N. Gajjar · R. K. Digavalli (✉)
Department of Mechanical Engineering, Indian Institute of Technology Delhi, New Delhi, India
e-mail: dravi@mech.iitd.ac.in

B. Modi
Department of Mechanical Engineering, Nirma University, Ahmedabad, India

Introduction

The failure in sheet metal forming is often preceded by the onset of localized necking, which can be represented by forming limits or limit strains, determined by elaborate laboratory experiments. The measured strains are typically represented in terms of limiting principal strains, known as the forming limit diagram (FLD). The diagram was first constructed by Keeler and Goodwin, following the concept of Keeler and Backofen [1]. The FLD represents the onset of localized (visible) necking over all the possible combinations of strains in the plane of a sheet. The detailed procedure for determination of the FLD has been explained in several publications [2, 3]. Anisotropy and strain hardening exponent (n) have a significant influence on the level and shape of an FLD [4]. A high normal anisotropy ($\bar{R}$ value greater than 1 increases the FLD level on the left-hand side of the diagram and slightly depresses the FLD level on the right-hand side [5, 6]. Increase in the level on the left-hand side of the FLD indicates improved formability in drawing mode. It was shown that significant improvement in FLD level can be obtained by using thicker sheets and sheets with higher n value, particularly in the biaxial stretching region [7].

Effect of Pre-strain and Strain Path Unfold

Variations in the pre-strain and strain path have a profound effect on the limit strains and consequently on the forming limit diagrams. Ghosh and Laukonis [8] experimentally determined the path-dependent nature of a strain-based FLD. Forming limits of cold rolled, aluminum-killed steel of 0.89 mm thickness with different pre-strain values (3.1%, 6.7% and 11.9%) in equi-biaxial tension were

measured. It was observed that the shape and location of FLDs change with increase in pre-strain value. Graf and Hosford [9] determined forming limit diagrams of Al-alloys after pre-straining to several levels in uni-axial, biaxial and plane-strain tensions in directions parallel and perpendicular to the rolling direction. It was concluded that pre-straining in biaxial tension decreases formability, while pre-straining in uni-axial tension and plane-strain raises the forming limits for subsequent strain combinations. Graf and Hosford [10] observed change in strain path due to pre-strain in uni-axial, equi-biaxial and near-plane-strain tension. The strain-based forming limit diagram was plotted for Al 2008 T4 in the as-received condition as well as with pre-strain. From the FLDs plotted for biaxial pre-strain values of 0.04, 0.07, 0.12 and 0.17, tested in a direction perpendicular to the rolling direction, it was observed that the shape and location of FLDs changed with different kinds of pre-strain.

Stress-Based FLDs

As discussed above, strain-based FLDs are not reliable for predicting sheet metal failure if there is a change in strain path. In view of this, Stoughton [11, 12] introduced the concept of stress-based FLDs. It was shown that the strain-based FLD (ε-FLD) can be transformed into stress-based FLD (σ-FLD) by using Hills's 1948 theory for plastic potential of a material with in-plane isotropy and a simple power law for stress–strain relation. All 15 curves of Graf and Hosford [10] transformed into stress state. These curves can be represented by a single curve as relative variations in stress-based FLDs are approximately five times smaller than relative variation in strain-based FLDs. Thus, all strain-based FLDs could be defined by a single curve in stress space, which is called the stress-based FLD. A single curve in stress space indicates the path independent nature of stress-based FLDs as well as insensitiveness to magnitude and nature of pre-strain (biaxial, uni-axial, plane strain) [13]. Chen et al. [14] applied a stress-based FLD suggested by Stoughton [11] in numerical simulation of multi-step stamping and found that finite element simulation results are in good agreement with that of experimental data. Zhou et al. [15] tested forming limits of an aluminum alloy and determined the strain-based FLD experimentally. The strain-based FLD was transformed into stress-based FLD by using the Stoughton approach. This stress-based FLD was then used in conjunction with LS-DYNA finite element simulation to predict the failure location in tube hydroforming. Sing and Rao [16] proposed a methodology for obtaining stress-based forming limit diagrams directly from readily measurable material properties by a simple tensile test. Instead of converting strain-based FLD into stress-based FLD by following the Stoughton approach, the stress-based FLD was obtained directly by using material properties such as strain hardening coefficient n, strength coefficient k, normal anisotropy ($\bar{R}$) and ultimate tensile stress. These properties are calculated from simple tensile tests. Obtaining the stress-based FLD without the strain-based FLD is a great advantage, as determining a strain-based FLD experimentally is a tedious and time-consuming task.

In most of the numerical studies, it is observed that the conventional strain-based forming limit diagrams (FLDs) have been used for the prediction of failure. The strain-based FLDs in the FE software are predicted using some empirical relations which correlate plain strain FLD with strain hardening index (n) and material thickness (t), initially proposed by Keeler [17]. But these formulae have not been found to be suitable for aluminum alloys. In addition, these strain-based FLDs are valid for cases where there is no change in strain path. But, because of change in strain path due to initial drawing and then biaxial stretching at the corners in hydroforming of a square-shaped part, it could lead to erroneous prediction of failure. The nature and magnitude of pre-strain also affect the accuracy of predicted results when a strain-based FLD is used. No attempts have been made in the past to predict failure in sheet hydroforming of deep-drawn cups using σ-FLDs. Also, σ-FLDs were determined using Hill's quadratic and non-quadratic yield criteria only. The yield function proposed by Barlat and Lian [18] has been shown to be particularly suitable for aluminum alloys. In view of the above, the present work is aimed at the development of σ-FLDs using Barlat's three-parameter plasticity model and prediction of failure in FE simulations of hydroforming of square cups from an automotive-grade aluminum sheet (AA5182) using the developed stress-based FLD followed by experimental validation of the same.

Development of Stress-Based FLD from Strain-Based FLD

Using Hill's Quadratic Yield Criterion

Hill's quadratic yield criterion considering anisotropic plastic potential is used for homogeneous material characterized by three orthogonal axes of anisotropy x, y and z. This yield criterion is used for determining yielding behavior of a rolled sheet having both normal and planar anisotropy.

The Hill's quadratic yield function has the following form [19]

$$2f(\sigma_{ij}) = F(\sigma_y - \sigma_z)^2 + G(\sigma_z - \sigma_x)^2 + H(\sigma_x - \sigma_y)^2 + 2L\tau_{yz}^2 + 2M\tau_{zx}^2 + 2N\tau_{xy}^2 = 1 \quad \text{(Eq 1)}$$

where F, G, H, L, M and N are constants which characterize the anisotropy.

The analytical procedure to transform the strain-based FLD into stress-based FLD using Hill's theory of yielding and a simple power law for plastic stress–strain relation has already been published [11, 12] and hence not elaborated here. This procedure has been used in the present work to develop a stress-based FLD of AA 5182 alloy sheets.

Using Barlat's Yield Function (1989)

In the present work, yield function proposed by Barlat and Lian [18] has also been used to convert the strain-based FLD into a stress-based FLD by modifying Stoughton's analytical procedure.

Barlat and Lian [18] introduced coefficients (a, c, h and p) into the plane stress yield function proposed by Barlat and Richmond [20] to characterize anisotropy, and it is given as follows.

$$f = a|K_1 + K_2|^M + a|K_1 - K_2|^M + c|2K_2|^M = 2(\overline{\sigma})^M \quad \text{(Eq 2)}$$

where

$$K_1 = \frac{\sigma_{xx} + h\sigma_{yy}}{2} \quad \text{and}$$

$$K_2 = \sqrt{\left(\frac{\sigma_{xx} - h\sigma_{yy}}{2}\right)^2 + p^2\sigma_{xy}^2}$$

a, c and h can be calculated using anisotropic parameters R_0 and R_{90} as follows.

$$a = 2 - c = 2 - 2\sqrt{\frac{R_0}{(1+R_0)}\frac{R_{90}}{(1+R_{90})}}$$

$$h = \sqrt{\frac{R_0}{1+R_0}\frac{1+R_{90}}{R_{90}}}$$

M is Barlat's exponent. For face-centered cubic (FCC) materials such as aluminum alloys, the most suitable value of M is 8.

Sheet metal is considered to be an orthotropic material with principal axes aligned with length, width and thickness. Taking x, y and z as principal axes for orthotropic material and putting $\sigma_3 = 0$ for a thin sheet subjected to plane stress conditions, from Eq 2, we get:

$$f = a|\sigma_1|^M + a|h\sigma_2|^M + c|\sigma_1 - h\sigma_2|^M = 2(\bar{\sigma})^M \quad \text{(Eq 3)}$$

So, effective stress is given by

$$\bar{\sigma} = \left(\frac{1}{2}\left(a|\sigma_1|^M + a|h\sigma_2|^M + c|\sigma_1 - h\sigma_2|^M\right)\right)^{\frac{1}{M}} \quad \text{(Eq 4)}$$

Ratio of effective stress $\overline{\sigma}$ to major principal stress (σ_1) is given by

$$\xi = \frac{\overline{\sigma}}{\sigma_1} = \left(\frac{1}{2}\left[a + a|h\alpha|^M + c|1 - h\alpha|^M\right]\right)^{1/M} \quad \text{(Eq 5)}$$

By differentiating Eq 4 with respect to σ_1 and σ_2, we can get the corresponding strains given as follows:

$$d\varepsilon_1 = M\left[a|\sigma_1|^{M-1} + c|\sigma_1 - h\sigma_2|^{M-1}\right] \quad \text{(Eq 6)}$$

$$d\varepsilon_2 = M\left[a|h\sigma_2|^{M-1} - ch|\sigma_1 - h\sigma_2|^{M-1}\right] \quad \text{(Eq 7)}$$

The strain ratio (β) is given by:

$$\beta = \frac{d\varepsilon_2}{d\varepsilon_1} = \frac{a|h\alpha|^{M-1} - ch|1 - h\alpha|^{M-1}}{a + c|1 - h\alpha|^{M-1}} \quad \text{(Eq 8)}$$

Stress ratio (α) can be obtained iteratively from the above equation for each known value of β. The steps to determine σ-FLD from ε-FLD are as follows.

1. From the experimental FLD (plotted with true strains), get true strain ratio β for each point on the FLD.
2. Obtain values of stress ratio (α) iteratively for each value β by using Eq 8.
3. Obtain values of ξ by putting the calculated value of α in Eq 5.
4. Using the values of β, α and ξ, obtain effective strain by [19]:

$$\overline{\varepsilon} = \varepsilon_1\left(\frac{\sigma_1}{\overline{\sigma}}\right)(1 + \alpha\beta) \quad \text{(Eq 9)}$$

5. Obtain effective stress by using Hollomon's equation, $\overline{\sigma} = k\overline{\varepsilon}^n$.
6. Obtain major and minor stresses by using the following relations:

$$\sigma_1 = \frac{\overline{\sigma}}{\xi},$$

$$\sigma_2 = \alpha\sigma_1$$

A MATLAB code has been developed to calculate the values of σ_1 and σ_2 for different values of strain combinations on the strain-based FLD. The major principal stress versus minor principal stress curve is plotted to get the stress-based FLD. For the AA5182 alloy sheet used in the present work, the experimentally determined strain-based FLD and the calculated stress-based FLD are shown in Fig. 1 and Fig. 2, respectively.

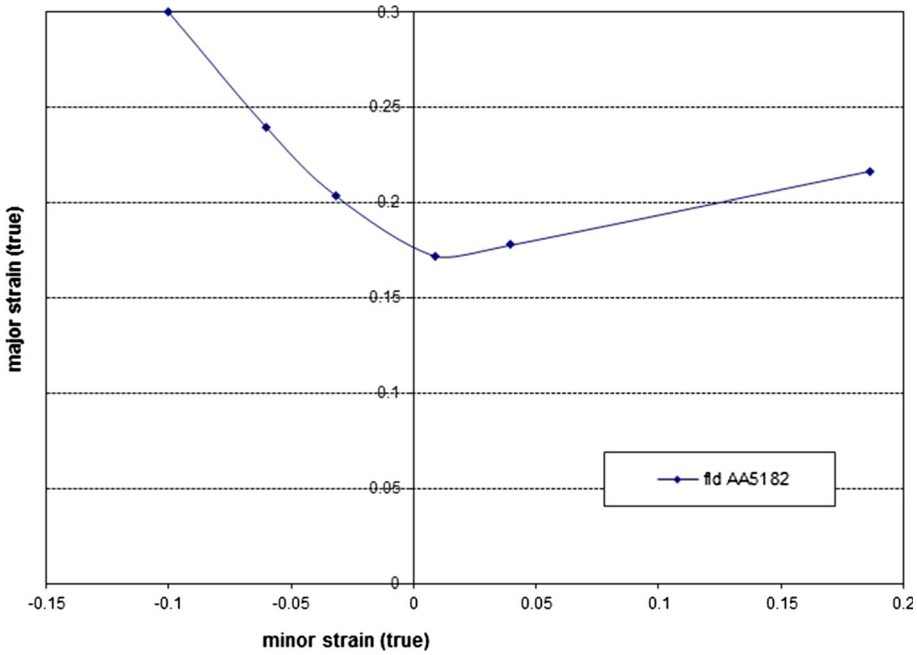

Fig. 1 Experimentally determined strain-based FLD of AA5182 sheets

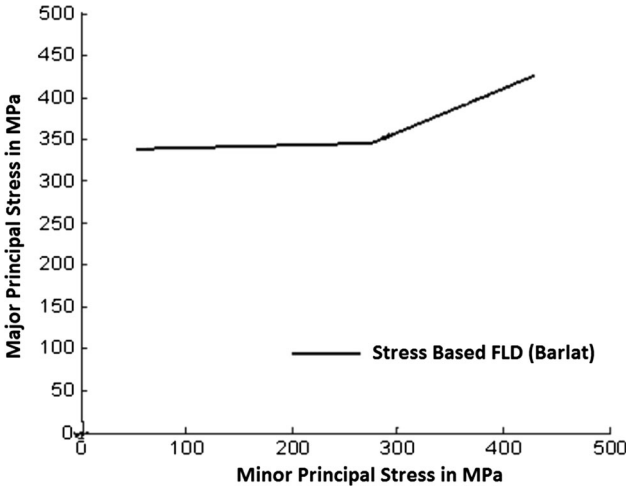

Fig. 2 Stress-based FLD of AA5182 alloy developed from the strain-based FLD using Barlat's yield model

Numerical Simulation of Hydroforming of Square Cups and Experimental Validation

Sheet hydroforming involves the application of high fluid pressure, usually through the blank holder, to form the blank into the shape of the die cavity. Hydroforming processes have been developed to improve the material formability and the accuracy of the formed part, and to reduce the number of forming steps. Numerical simulation of hydroforming of square cups has been carried out using finite element method to evaluate the influence of process variables on formability (success/failure) of AA5182 alloy with the help of commercially available code LS-DYNA (version 971).

The tools (die and blank holder) were modeled and were considered as rigid bodies neglecting the very little elastic deformation during hydroforming. Triangular and rectangular thin shell elements were used to mesh the parts. The model of the targeted part and a typical FE model of the tools and the blank (with the dimensions) used for simulation of sheet hydroforming of a 35 mm deep square cup are shown in Fig. 3. A square blank of 166 mm side with a corner radius of 70 mm was modeled with five integration points through the thickness using Gauss rule with 1 mm initial blank thickness. For better computational accuracy, a fine mesh was used and the average element size of the blank mesh was 3 mm. Tensile properties and anisotropic parameters of the alloy (given in Table 1), determined from the tensile tests, were given as input to define the material behavior during plastic deformation. The coefficient of friction at the contact between the blank and the die was taken as 0.04 for the lubricated condition [21]. The pressure boundary condition was applied at all the nodes on the blank within the area confined by a line as shown in Fig. 3. This line represents the die cavity in which the fluid pressure was applied. FE simulations were performed with variable pressure-blank holding force (BHF) load path. The pressure was gradually increased to a predetermined peak value (in the range of 22–24 MPa), and the BHF was applied in the range of 10–30 kN in addition to the minimum closing force required to prevent leakage of the fluid.

To validate the numerical predictions, an experimental setup was designed for deep-drawing of square cup-shaped

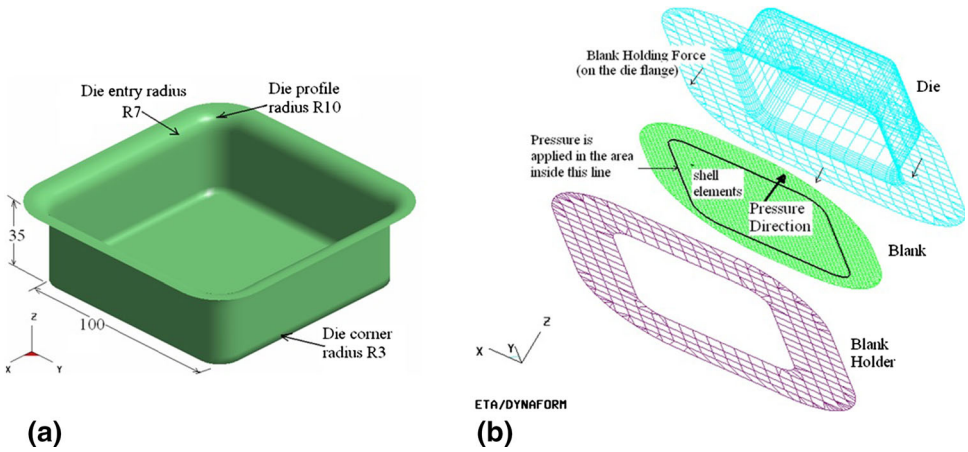

Fig. 3 (**a**) Dimensions of the targeted part and (**b**) FE model used for simulation of hydroforming

Table 1 Mechanical properties and anisotropic parameters of AA 5182 sheets

Angle wrt RD (degree)	YS (MPa)	UTS (MPa)	% Elongation	Strain hardening index *n*	Strength coefficient *K* (MPa)	Anisotropic parameter *R*
0	161.8	295.0	18.0	0.35	635.1	0.75
45	145.3	273.0	19.6	0.36	577.2	0.90
90	157.5	283.8	18.8	0.35	589.4	0.82
Average	152.5	281.2	19.0	0.35	594.8	0.84 ($\bar{R}$)
Standard deviation	8.5	11.0	0.8	0.004	30.5	0.08

wrt with respect to; *RD* rolling direction

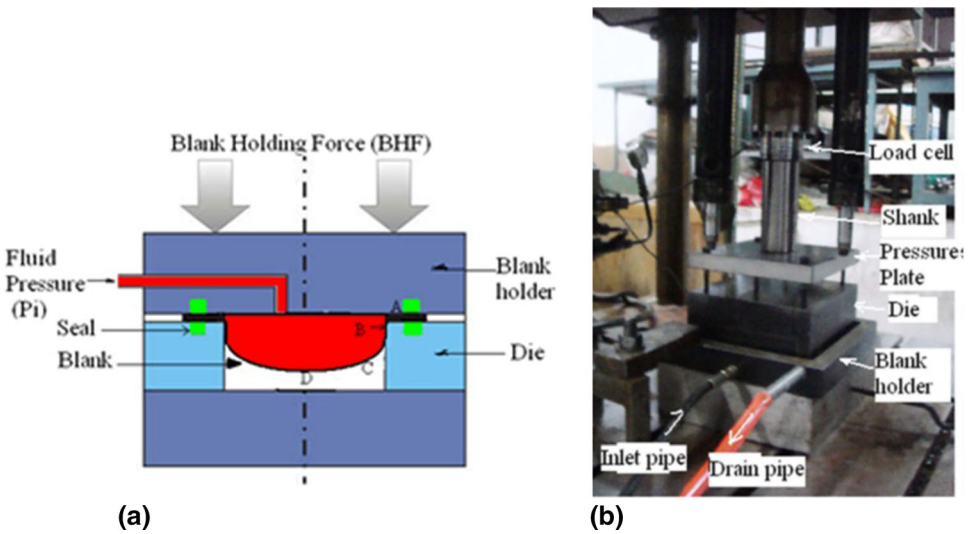

Fig. 4 (**a**) A schematic and (**b**) the actual experimental setup for deep-drawing of square cups by hydroforming

parts by hydroforming of AA 5182 sheets as shown in Fig. 4 [22].

Failure Prediction Using Stress-Based FLDs

Formability of the sheets was first predicted in FE simulation using the strain-based FLD generated in the post-processor of the software as shown in Fig. 5a. The FLD, plotted using Keeler's formula of FLD_0 (a function of thickness t and strain hardening exponent *n*), overestimated the limit strains of the Al alloy. Therefore, the maximum strains in the part are well below the FLD indicating a successful forming. However, failure was observed at one of the corners in the cup in the experiments as shown in Fig. 5b. Therefore, for better prediction, experimentally determined strain-based FLD of AA5182 was used as an input to the software to predict the failure. Major and minor

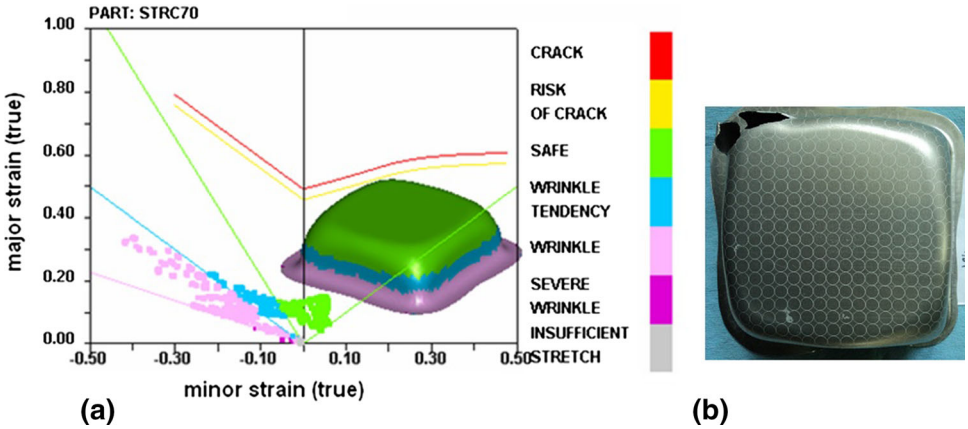

Fig. 5 (**a**) Formability prediction by FE method using strain-based FLD generated in the post-processor (peak pressure 23.5 MPa and BHF 30 kN) and (**b**) experimentally formed cup with peak pressure 23.5 MPa and BHF 30 kN showing fracture at one of the corners

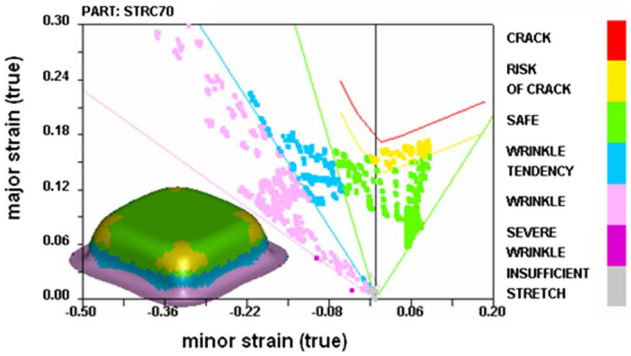

Fig. 6 Failure prediction by FE method using experimental strain-based FLD (peak pressure 23.5 MPa and BHF 30 kN)

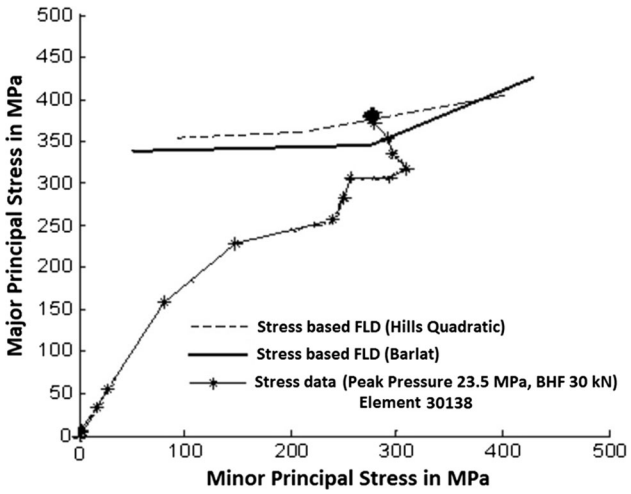

Fig. 7 Failure prediction by stress-based FLDs (peak pressure 23.5 MPa and BHF 30 kN)

strains in the cups predicted in FE simulation were superimposed on the experimental ε-FLD as shown in Fig. 6. The strains in the corner region of the cup were found to be in the critical region (just below the FLD), but no failure was predicted.

Stress-based FLDs developed using both Hill's quadratic and Barlat's yield models were also used for failure prediction. Major and minor principal stresses of the element (number 30138) in the corner region have been captured from the FE simulation and superimposed on the σ-FLD (as shown in Fig. 7) with the help of the MATLAB code. The stress path of the element in the diagram exceeds the σ-FLD line, and it clearly indicates failure in the cup which is consistent with the experimental result. The strain path of an element from the corner of the cup, as shown in Fig. 8, clearly shows the change in strain path from plane-strain toward biaxial stretching and again to plane-strain mode of deformation (increase in major strain with constant minor strain). It is consistent with the stress pattern exhibited by the same element in the σ-FLD. The stress path of this element initially showed biaxial tensile stresses, reached equi-biaxial stretching and crossed the σ-FLD with a sudden rise in the major stress. Stress-based FLD (σ-FLD) developed by using Hill's quadratic yield model was also imported into this code for comparison of accuracy of failure prediction. Though both predicted failure, as observed in Fig. 7, σ-FLD with Barlat's model predicts slightly lower limiting stresses than the σ-FLD with Hill's quadratic yield criterion, and hence it is safer to use the σ-FLD with Barlat's model.

Formability of a cup hydroformed with 23.5 MPa peak pressure and 10 kN BHF (in excess to the closing force just required to prevent leakage of the fluid) has been predicted. The cup was successfully formed experimentally as shown in Fig. 9.

FE simulation using experimental ε-FLD as the failure criterion predicts the strain at the corner in the risk of failure zone (Fig. 10), i.e., between forming limit curve and safe margin line. This indicates that the cup may or may not be hydroformed successfully. Superimposition of principal stresses of an element (number 31121) from the corner region on the σ-FLD, shown in Fig. 11, accurately

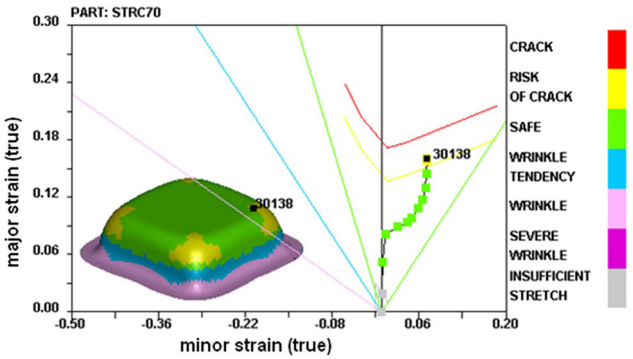

Fig. 8 Strain path of an element at the corner (peak pressure 23.5 MPa and BHF 30 kN)

Fig. 9 Square cup hydroformed with 23.5 MPa peak pressure and 10 kN BHF

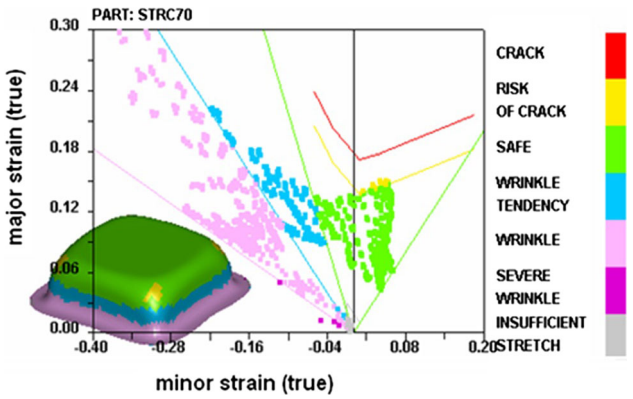

Fig. 10 Formability prediction by FE method using strain-based FLD (peak pressure 23.5 MPa, BHF 10 kN)

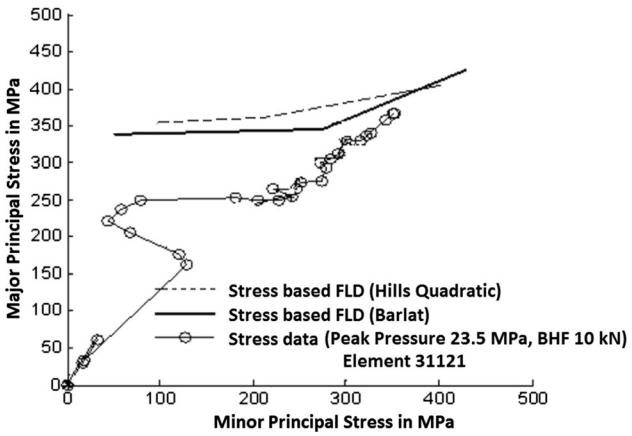

Fig. 11 Failure prediction by stress-based FLD (peak pressure 23.5 MPa, BHF 10 kN)

predicts successful forming of the cup, which is consistent with the experimental result.

Though the principal stresses of the element are higher than that of element in the previous case (with 30 kN BHF), the cup could be formed successfully. This can be attributed to higher forming limits in equi-biaxial stretching mode as the material at the corner has undergone deformation under equi-biaxial stretching toward the end of forming (in the calibration stage), as shown in Fig. 12.

In both of the above cases, failure prediction with the σ-FLD has been found to be more accurate than the prediction with ε-FLD. This can be attributed to the change in strain path at the four bottom corners of the part which are the most critical regions due to maximum deformation there. As illustrated in Fig. 13a, in the hydroforming process, the blank bulges out initially due to fluid pressure. The blank deforms under pure stretching mode at the pole region and deep-drawing mode in the flange region simultaneously till the sheet bulges out to the depth of the die. In the next stage, drawing-in of the sheet continues without any stretching at the pole. Finally, corners are

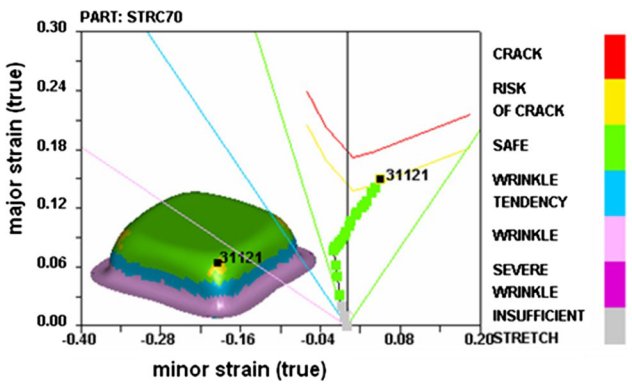

Fig. 12 Strain path of an element at the corner (peak pressure 23.5 MPa, BHF 10 kN)

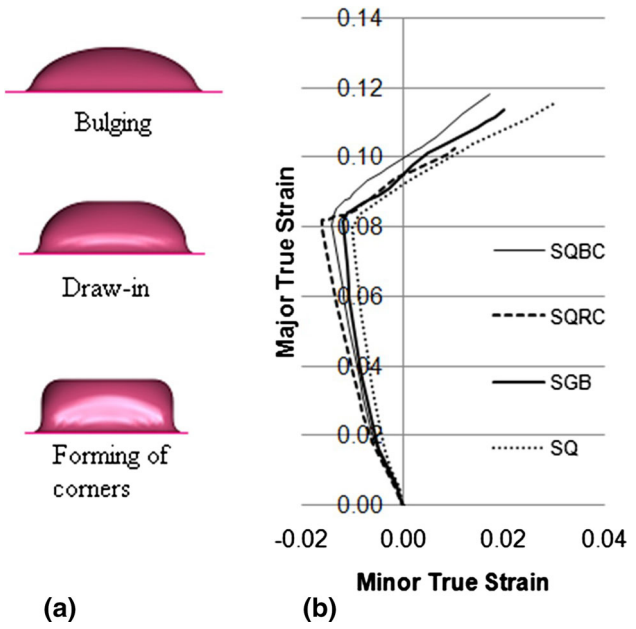

Fig. 13 (**a**) Different stages in square cup hydroforming and (**b**) strain path change at the corner for blanks of different shapes

formed under pure stretching mode of deformation. The change in strain path of an element at the corner in blanks of different shapes is also shown in Fig. 13b. The different shapes of blanks used are square blank (SQ), modified square blank as predicted by blank size estimator in the FE program (SQB), square blank with rounded corners (SQRC) and square blank with beveled corners (SQBC).

Moreover, deformation during the initial stage can be considered as pre-strain for subsequent biaxial stretching in the corners. Shift in size and location of ε-FLD was also reported with the pre-strain [9]. Thus, the corner region with initial pre-strain exhibits change in strain path, and for accurate prediction of formability, a modified strain-based FLD is required. However, as explained earlier, strain-based FLDs with different pre-strain levels can be represented by a single curve in the stress space, and the σ-FLD has been found to predict failure more accurately in the case of hydroforming of square cups.

Conclusions

In this work, stress-based FLDs have been developed from strain-based FLDs using two different yield criteria (Hill's quadratic and Barlat's three-parameter model) and used in prediction of failure in FE simulations of hydroforming of square cups from AA5182 alloy sheets. The stress-based FLD with Barlat's model predicts slightly lower limiting stresses than with Hill's quadratic yield criterion. A significant difference has been found in failure prediction between strain-based and stress-based criteria when they are applied to sheet hydroforming of square cups. Experimental work by increasing the fluid pressure to obtain fracture for a given blank holding force showed that the prediction by a stress-based forming limit diagram is more accurate. It is due to the change in strain path that has been observed at the corners in hydroforming of square cups, where the deformation mode changes from initial drawing to biaxial stretching during final calibration. This work clearly shows that accuracy in failure prediction can be improved in sheet hydroforming of cup-shaped parts with flat bottom by using stress-based forming limit diagram.

References

1. S.P. Keeler, W.A. Backofen, Plastic instability and fracture in sheets stretched over rigid punches. Trans. ASM **56**, 25–48 (1963)
2. S.S. Hecker, A Simple technique for determining forming limit curves. Sheet Metal Ind **52**(11), 671–676 (1975)
3. A.K. Ghosh, S.S. Hecker, Failure in thin sheets stretched over rigid punches. Metall. Trans. A **6**, 1065–1073 (1975)
4. P.B. Mellor, Sheet metal forming. Int. Met. Rev. **26**, 1–20 (1981)
5. Z. Marciniak, K. Kuczynski, T. Pokora, Influence of the plastic properties of a material on the forming limit diagram for sheet metal in tension. Int. J. Mech. Sci. **15**, 789–805 (1973)
6. S.E. Jones, P.P. Gillis, A generalised quadratic flow law for sheet metals. Met. Trans. A. **15**, 133–138 (1984)
7. J. Hiam, A. Lee, Factors influencing the forming limit curves of sheet steel. Sheet Metal Ind. **55**, 631–643 (1978)
8. Ghosh, A.K., and Laukonis, J.V.: The influence of strain-path changes on the formability of sheet steel, in 9th Biennial Congress of the International deep drawing research group, sheet metal forming and energy conservation (ASM Publication, 1976)
9. A. Graf, W.F. Hosford, Calculations of forming limit diagrams for changing strain paths. Metall. Trans. A **24**, 2497–2501 (1993)
10. A. Graf, W. Hosford, The influence of strain-path changes on forming limit diagrams of A16111-T4. Int. J. Mech. Sci. **36**, 897–910 (1994)
11. T.B. Stoughton, A general forming limit criterion for sheet metal forming. Int. J. Mech. Sci. **42**, 1–27 (2000)
12. T.B. Stoughton, Stress-based forming limits in sheet metal forming. J. Eng. Mater. Technol. **123**, 417–422 (2001)
13. T.B. Stoughton, Z. Xinhai, Review of theoretical models of the strain-based FLD and their relevance to the stress-based FLD. Int. J. Plast. **20**, 1463–1486 (2004)
14. M.H. Chen, L. Gao, D.W. Zuo, M. Wang, Application of the forming limit stress diagram to forming limit prediction for the multi-step forming of auto panels. J. Mater. Process. Technol. **187–188**, 173–177 (2007)
15. L. Zhou, K.M. Xue, L. Ping, Determination and application of stress-based forming limit diagram in aluminum tube hydroforming. Trans. Nonferrous Met. Soc. China **17**, 21–26 (2007)
16. W.M. Sing, K.P. Rao, Prediction of sheet-metal formability using tensile-test results. J. Mater. Process. Technol. **37**, 37–51 (1993)
17. S.P. Keeler, Understanding sheet metal formability. Sheet Metal Ind. **48**, 357–364 (1971)
18. F. Barlat, J.I. Lian, Plastic behavior and stretchability of sheet metals, Part-I. Int. J. Plast. **5**, 51–56 (1989)
19. W.F. Hosford, R.M. Caddell, *Metal forming: mechanics and metallurgy* (Cambridge Press, New York, 1993)

20. F. Barlat, O. Richmond, Crystallographic texture, anisotropic yield surfaces and forming limits of sheet metals. Mat. Sci. Eng. **91**, 55–72 (1987)
21. K.P. Rao, C.L. Xie, A comparative study on the performance of boric acid with several conventional lubricants in metal forming processes. Tribol. Int. **39**, 663–668 (2006)
22. B. Modi, D. Ravi Kumar, Development of a hydroforming set up for deep drawing of square cups with variable blank holding force technique. Int. J. Adv. Manuf. Technol. **66**, 1159–1169 (2013)